FARADAY

Study of strongly overlapping Rh^{2+} EPR spectra by high-resolution magnetic resonance techniques†

Kris Sabbe,‡[a]* Henk Vrielinck,[a] Freddy Callens,§[a] Etienne Boesman,[a] Hans Vercammen,‡[b] Hanno Käß,[b] Etienne Goovaerts,[b] August Bouwen[b] and Dirk Schoemaker[b]

[a] *Laboratory for Crystallography and Study of the Solid State, Krijgslaan 281-S1, B-9000 Ghent, Belgium*
[b] *University of Antwerp (UA) Department of Physics, Universiteitsplein 1, B-2610 Antwerp, Belgium*

Received 23rd April 1998, Accepted 11th June 1998

Recent EPR and ENDOR publications demonstrated that several closely related Rh^{2+} complexes may be simultaneously present in rhodium doped NaCl and AgCl. These complexes only differ with respect to vacancy compensation. They exhibit strongly overlapping X-band EPR spectra with $g_{\perp} \approx 2.5$ and $g_{\parallel} \approx 2$. In the present study, solution- and melt-grown NaCl single crystals doped with Rh^{3+} were subjected to several treatments, such as X-irradiation, heating and thermal pulse annealing. While X-band EPR alone has insufficient resolution to resolve the spectra of the various rhodium complexes, a combined X-band ENDOR and W-band EPR study allows a consistent spectrum decomposition and interpretation. The X- and W-band Rh^{2+} spectra of both solution- and melt-grown NaCl single crystals are discussed in terms of the same $[RhCl_6]^{2-} \cdot n$vac ($n = 0, 1, 2$) complexes.

Introduction

The subject of the present study is the characterisation of cation dopants in photographic AgX (X = Cl, Br) emulsions and related materials. Electron paramagnetic resonance (EPR) and electron nuclear double resonance (ENDOR) are important tools to investigate the microscopic structure of such paramagnetic metal ion complexes in many host materials. Especially with ENDOR, detailed information on the complex and its lattice surroundings can be obtained using the anisotropy of the hyperfine and quadrupole interactions of the neighbouring magnetic nuclei. Both methods, EPR and ENDOR, are favourably applied to single crystals. It is, however, not always possible to grow large single crystals, *e.g.* no large solution-grown AgX single crystals that are fully comparable with photographic AgCl emulsions are available. From a comparative study between EPR and ENDOR results in AgX single crystals and powders it appeared that powder ENDOR of AgX emulsions is feasible, though not simple.[1,2] Large AgX single crystals, however, can easily be grown from the melt (Bridgman method) and are used as model-systems for AgX emulsion powders.[3–9] Because the metal ion complexes in solution- and melt-grown crystals can be different, especially when ligand exchange is considered, large NaCl solution- and melt-grown single crystals are also used as model-systems.[9–16]

From the EPR and ENDOR study of large solution- and melt-grown NaCl and AgCl crystals and powders, several rhodium-related spectra have been detected and assigned to Rh^{2+} complexes.[1–4,7–15] In most cases this was only possible after choosing the pretreatment and the recording conditions to isolate and identify the individual spectra. In spite of the fact that important progress has been made, certain assignments are somewhat speculative and a few questions remained unanswered, especially if the only possibility is to study the samples under conditions where several strongly overlapping Rh^{2+} spectra are simultaneously present. In that case X-band EPR is often insufficient to monitor the presence and relative contributions of the individual spectra. Therefore, in the present study, magnetic resonance techniques with higher resolution, *i.e.* X-band ENDOR and W-band EPR, were used. It will be shown that the assignment of the EPR and ENDOR spectra is consistent for both solution- and melt-grown NaCl crystals and the consequences for AgCl melt-grown crystals and solution-grown powders will be discussed.

Review of rhodium-related paramagnetic centres in NaCl and AgCl

In Table 1 the different rhodium complexes presently known in the three model systems and in AgCl emulsion powders are listed. The O(I) complex is elongated along the [001] axis and is identified as having two next-nearest neighbour (nnn) charge compensating Na^+ vacancies, arranged in such a way that the Rh-vacancy axes are orthogonal in the plane perpendicular to the symmetry axis of the complex [Fig 1(a)]. This overcompensated complex has orthorhombic-I symmetry, with principal g-tensor axes along [110], [1$\bar{1}$0] and [001].[12–13] The O(II) complex has only one cation vacancy in a nnn position, in the plane perpendicular to the elongation axis [Fig. 1(b)]. The O(II) complex is fully charged compensated and the symmetry is orthorhombic-II (principal g-tensor axes are along cubic crystal axes).[9,13,14] A third $[RhCl_6]^{4-}$ complex, called RTAX, is identified as a non-locally charge compensated axial defect also elongated along its [001] axis [Fig. 1(c)].[10,13] These three defects [O(I), O(II) and RTAX] have the same surrounding nuclei and only differ with respect

† Presented at the 31st International Meeting of the ESR Group of the Royal Society of Chemistry, University of Manchester, 1998.

‡ Financially supported by the Flemish Institute for the Encouragement of Scientific and Technological Research in Industry (IWT).

§ Research Director of the Fund for Scientific Research, Flanders, Belgium.

Table 1 Occurrence of different rhodium complexes in photographic emulsions and three model systems: NaCl solution-grown, NaCl melt-grown and AgCl melt-grown single crystals

NaCl solution-grown	NaCl melt-grown	AgCl melt-grown	AgCl emulsion
$[RhCl_6]^{4-} \cdot 2vac$ O(I) refs. 12, 13	$[RhCl_6]^{4-} \cdot 2vac$ O(I) refs. 9, 14 this study	$[RhCl_6]^{4-} \cdot 1vac$ O(II)-like ref. 3	$[RhCl_4X_2]^{2-}$ $(X = H_2O)$ R4 ref. 1
$[RhCl_6]^{4-} \cdot 1vac$ O(II) ref. 13	$[RhCl_6]^{4-} \cdot 1vac$ O(II) refs. 9, 14,		$[RhCl_5X]^{3-}$ $(X = H_2O)$ R5 ref. 1
$[RhCl_6]^{4-} \cdot 0vac$ RTAX refs. 10, 13	$[RhCl_6]^{4-} \cdot 0vac$ RTAX this study		$[RhCl_6]^{4-}$ R6 refs. 1, 2
$[RhCl_5X]^{n-}$ $(X = OH^-$ $(n = 4)$ or H_2O $(n = 3)$ B-centre refs. 10, 11, 13	Rh-dimer refs. 9, 14, 15		
Rh^+ ref. 16	Rh (axial) refs. 9, 14		

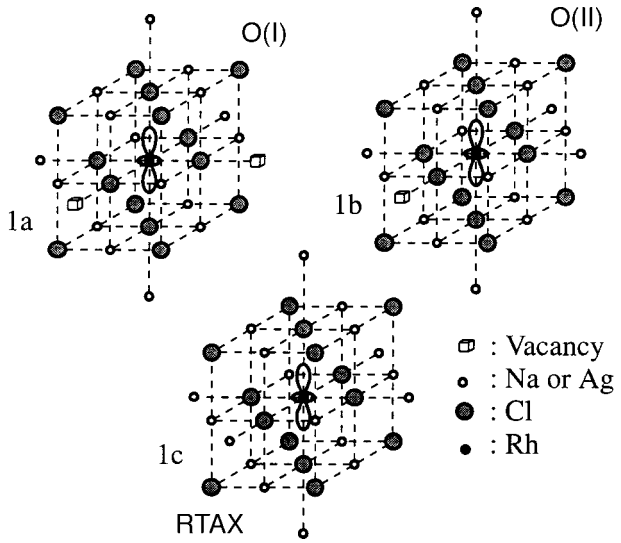

Fig. 1 O(I) (a), O(II) (b) and RTAX (c) Rh^{2+} ion with its nearest neighbours in NaCl and AgCl.

to vacancy compensation. Because the g-values of O(I), O(II) and RTAX, are very close (Table 2), the X-band EPR spectra are strongly overlapping.

In addition to these three centres, two more defects have been detected in solution-grown NaCl crystals. The first defect can only be observed with ENDOR at very low temperatures ($T < 15$ K) and is assigned to a cubic Rh^+ defect, having the same environment as RTAX.[16] The second defect, labelled the B-centre, was tentatively identified as a $[RhCl_5X]^{n-}$ $[X = OH^-$ $(n = 4)$ or H_2O $(n = 3)]$ complex.[10]

In the melt-grown NaCl single crystal, in addition to O(I), O(II) and RTAX, a fourth rhodium-related defect is identified as a rhodium dimer,[9,14,15] but a fifth axial rhodium complex remains unidentified.[9,14]

The primary defect in the melt-grown AgCl single crystal has an orthorhombic-II symmetry and its structure is identical to that of the O(II) complex in the solution- and the melt-grown NaCl single-crystal.[3] The similarity between the g-values in both NaCl and AgCl demonstrates that NaCl can indeed be used as a model system for AgCl (Table 2). In the AgCl emulsion, X-irradiated at room temperature, three Rh^{2+} complexes are observed,[1,2] labelled R4, R5 and R6. The g-values of R6 are very close to those of the O(II)-like complex in the melt-grown AgCl single crystal.[1,2] R4 and R5 are thought to be hydrated complexes, similar to the B-centre in NaCl solution-grown crystals.[1,17]

Experimental

Materials

Rhodium doped NaCl single crystals were grown at room temperature by slow evaporation of a saturated aqueous solution of NaCl (Suprapur, Merck) containing 0.6 wt.% $Na_3RhCl_6 \cdot 12H_2O$ (Agfa-Gevaert N.V.). Because of the cubic structure of NaCl the crystals could be cleaved parallel to {100} planes and be easily oriented. The melt-grown NaCl crystals in this study were grown by using the Bridgman method by mixing Ultrapure NaCl with 0.8 wt.% of the same dopant.

Methods

The EPR and ENDOR spectra were recorded using a Bruker ESP300 X-band spectrometer with an ESP353E ENDOR/TRIPLE extension (EN374 RF amplifier with a maximum of 200 W, EN525 Schomandl synthesizer). The low temperatures were realised using an Oxford ESR10 cryostat. In our specific configurations designed to use large sample volumes, temperatures between 6 K and room temperature could be realized. The 95 GHz ESR measurements were done using a Bruker W-band spectrometer, equipped with an Oxford 6T superconducting magnet on a rotating base (University of Antwerp). The irradiation of the samples was performed using a Philips tungsten anticathode X-ray tube, operated at 60 kV and 40 mA.

Results and discussion

X-band EPR and ENDOR measurements were performed at 25 K. The W-band EPR spectra were taken at 20 K.

X-Band EPR

Solution-grown NaCl crystals. In the untreated NaCl solution-grown crystal no EPR signals are present. At first the crystal was irradiated at room temperature and measured immediately after irradiation. In the X-band EPR spectrum the presence of several Rh^{2+} defects can be observed [Fig. 2(a)].

Table 2 g-Tensors for O(I), O(II) and RTAX in three single crystals. The g-tensors are along the principal axes, unless stated otherwise. The number in parentheses indicates the error in the last digit.

Host	Complex	g_x	g_y	g_z	Ref.
NaCl solution-grown	O(I)[a]	2.4797(4)	2.4712(4)	2.0118(8)	13
	O(II)	2.4779(4)	2.4301(4)	2.0154(4)	13
	RTAX	2.4510(1)	2.4510(1)	2.0190(8)	10
NaCl melt-grown	O(I)[a]	2.4785(9)	2.4718(9)	–	This study
	O(II)	2.480(2)	2.431(2)	2.015(1)	14
	RTAX	2.448(3)	2.448(3)	–	This study
AgCl melt-grown	O(II)	2.426(2)	2.395(2)	2.011(1)	3

[a] Principal axes along [110], [1$\bar{1}$0], [001]

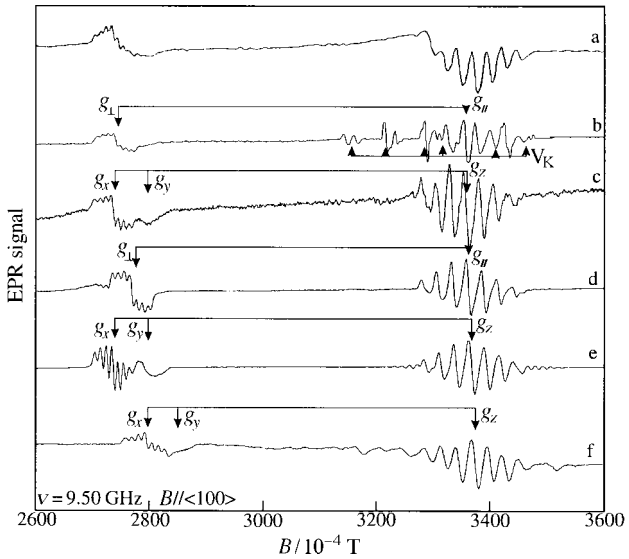

Fig. 2 X-Band EPR spectra of the solution-grown NaCl, the melt-grown NaCl and the melt-grown AgCl single crystal, doped with rhodium for B//⟨100⟩ at 25 K: (a) solution-grown NaCl crystal measured immediately after X-irradiation at room temperature, (b) solution-grown NaCl crystal measured after X-irradiation at liquid nitrogen temperature (LNT), (c) solution-grown NaCl crystal measured after X-irradiation at LNT and pulse-annealed to $T > 190$ K, (d) solution-grown crystal NaCl measured after X-irradiation at LNT and storage for a few days at room temperature, (e) melt-grown NaCl crystal before any treatment, (f) melt-grown AgCl crystal prior to any treatment.

When the solution-grown NaCl crystal is X-irradiated at liquid nitrogen temperature (LNT) for, typically, 20 min, only two paramagnetic centres are observed with X-band EPR [Fig. 2(b)]. Together with the well-known V_K centre,[18] signals of a first $[RhCl_6]^{4-}$ complex with nearly axial symmetry [O(I) Fig. 1(a)] are observed.[12,13] The V_K centres decay at 145 K. At that temperature the holes become mobile and can recombine with the Rh^{2+} centres.[13] In the thermal pulse-anneal experiments described below, the crystals were heated to a certain anneal temperature for typically 5 min and measured at the optimum detection temperature of 25 K. For annealing temperatures of $T > 190$ K the X-band EPR spectrum (at 25 K) changes mainly into the O(II) spectrum [Fig. 2(c)].[13] The g_x and g_z-values of the defect are almost identical to $g_\perp$ and $g_\parallel$ of the nearly axial O(I) defect (Table 2), and the formation of O(II) is revealed by the formation of its g_y component.[13] Finally, when the crystal is stored for a few days at room temperature, X-band EPR signals of a third $[RhCl_6]^{4-}$ complex are detected[10,13] [Fig. 2(d)]. The axial $[RhCl_6]^{4-}$ complex (RTAX) is also observed a few days after X-irradiation at room temperature. Because the g-values of these three defects are all very close (Table 2), the conversion from the nearly axial O(I) defect into the orthorhombic-II O(II) defect and finally to the axial RTAX defect is very difficult to monitor. The seven-line pattern around the g_x and g_z of the three complexes is due to the superhyperfine (SHF) interaction of the unpaired electron with the two equivalent axial chloride nuclei. No significant difference for the SHF values of these three defects was observed with EPR, which further complicates the evaluation of the X-band EPR spectra.

Melt-grown NaCl crystals. In the melt-grown NaCl crystal, in contrast to the solution-grown crystal, strong EPR signals are present without treatment. The rhodium is introduced as Rh^{3+} and during the growth the Rh^{3+} is reduced to Rh^{2+}. The EPR spectrum shows, besides the lines assigned to the Rh-dimer, clearly the presence of an orthorhombic-II $[RhCl_6]^{4-}$ centre [Fig. 2(e)].[9,14] It was shown that the latter defect is identical to the orthorhombic-II defect in the solution-grown NaCl crystal, and both are labelled O(II).[14] Neither heating, X-irradiating or pulse-annealing can remove the O(II) spectrum, and no X-band EPR signals of O(I) or RTAX are detected in the melt-grown NaCl crystal.[14]

Melt-grown AgCl crystals. Prior to any treatment in the AgCl melt-grown single crystal, clear signals are present from a $[RhCl_6]^{4-}$ centre with orthorhombic-II symmetry [Fig. 2(f)]. The X-band EPR spectra of this defect show a great similarity with the X-band EPR spectra of the O(II) complex in NaCl and it was obvious to propose the same structure for both defects [Fig. 1(b)].[3,9,14]

X-Band ENDOR and W-band EPR

The conversion from O(I) into O(II) and finally into RTAX for the solution-grown NaCl crystal. After X-irradiation at LNT the nearly axial O(I) complex is detected [Fig. 2(b)]. Prior to X-irradiation, a major part of the rhodium is present as the fully charge-compensated $[RhCl_6]^{3-}$ complex with the two nnn vacancies positioned as in O(I). The X-irradiation at LNT has reduced this fully charge-compensated Rh^{3+} complex to the paramagnetic O(I) complex, which is stable at these low temperatures because the vacancies are frozen in. Even if other Rh^{3+} configurations could exist, fully charge-compensated Rh^{3+} seems to be the most efficient, permanent electron trap at 77 K.

In Fig. 3(a) the corresponding ENDOR spectrum of the axial chloride nuclei for B//⟨100⟩ and $g = g_z$ is presented. As for every chloride isotope (^{35}Cl and ^{37}Cl, both $I = 3/2$) a pattern of six lines ($S = 1/2$, three $M_S = 1/2$ and three $M_S = -1/2$ transitions) is expected, all lines in Fig. 2(a) can be assigned, confirming that only O(I) is present. The analysis takes into account the ratios $A(^{35}Cl)/A(^{37}Cl)$ and $Q(^{35}Cl)/Q(^{37}Cl)$, 1.20 and 1.27, respectively, and the natural abundance of ^{35}Cl, which is three times larger than for ^{37}Cl.

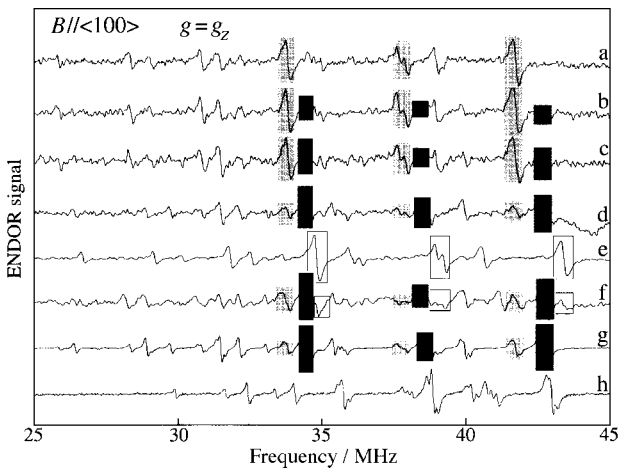

Fig. 3 X-Band ENDOR spectra of solution-grown NaCl, melt-grown NaCl and melt-grown AgCl single crystals doped with rhodium for B//⟨100⟩ and $g = g_z$ at 25 K for the axial chloride interaction. The dark rectangles correspond to the lines of O(II), the lighter rectangles to those of O(I) and the open rectangles to those of RTAX. Only the ^{35}Cl ($M_S = -1/2$) transitions are marked. (a) Solution-grown NaCl crystal measured after X-irradiation at LNT, (b) solution-grown NaCl crystal measured after X-irradiation at LNT and pulse-annealed for 5 min at $T = 190$ K, (c) solution-grown NaCl crystal measured after X-irradiation at LNT and pulse-annealed for 5 min at $T = 220$ K, (d) solution-grown NaCl crystal measured after X-irradiation at LNT and pulse-annealed for 5 min at $T = 240$ K, (e) solution-grown NaCl crystal measured after X-irradiation at LNT and storage for a few days at room temperature, (f) solution-grown NaCl crystal measured immediately after X-irradiation at room temperature, (g) melt-grown NaCl crystal prior to any treatment, (h) melt-grown AgCl crystal prior to any treatment.

In Fig. 3(b)–(d) the effect of increasing the annealing temperature on the ENDOR spectrum is illustrated: the number of lines is essentially doubled, indicating the gradual appearance of a second, similar spectrum, *i.e.* the O(II) spectrum. Whereas in X-band ENDOR the lines of O(I) and O(II) are nicely resolved, the O(I) X-band EPR spectra are totally covered by those of O(II) for each orientation of the magnetic field. The appearance of the O(II) spectrum and the accompanying loss of the vacancy from the O(I) centre is consistent with the increased mobility of the cation vacancies around 190 K.[19]

Increasing the annealing times, even at 240 K, cannot increase the ratio of the O(II) to the O(I) ENDOR intensities beyond approximately 3 : 1, indicating that an equilibrium between the O(II) and O(I) defects has been reached. In Fig. 4 the conversion is also depicted for the sodium and the rhodium interactions. As the natural abundances of ^{23}Na ($I = 3/2$) and ^{103}Rh ($I = 1/2$) are 100%, six and two lines for each interaction are expected, respectively. The six lines of the ^{23}Na interaction are centred around the nuclear Zeeman frequency of ^{23}Na, and in Fig. 4 only the $M_S = -1/2$ multiplet is marked.

When the crystal is stored for a few days at room temperature no more traces in X-band from O(I) and O(II) are observed, but a third, again very similar, $[RhCl_6]^{4-}$ ENDOR spectrum is observed [Fig. 3(e)], corresponding to the RTAX defect. With W-band EPR it is still possible to detect very small traces of O(I) and O(II).[13] Even at room temperature it is impossible to convert all O(I) defects into O(II) and finally into RTAX. Again roughly the same 3 : 1 ratio of the concentrations O(II) to O(I) is observed in the W-band spectra.

Returning to Fig. 3(f), the X-band ENDOR spectrum immediately after X-irradiation can be easily interpreted in terms of O(I), O(II) and RTAX contributions (3 sets of 12 lines). The intensity ratio between O(II) and O(I) is again roughly 3 : 1. Shortly after the X-irradiation only a minor part of O(I) and O(II) has been converted into RTAX. The presence of O(I) and O(II) is also confirmed by the angular variation of the rhodium interaction. As no ^{103} Rh interaction can be detected for RTAX, as was mentioned earlier,[10] the presence of this centre was monitored by the angular variation of the axial chloride interaction of the complex.

The presence of O(I) in the melt-grown NaCl single crystal. When considering again the ENDOR spectrum for $B//\langle 100\rangle$ and $g = g_z$ between 25 and 45 MHz (Fig. 3) we notice that in addition to the axial chloride interaction of O(II) a second axial chloride interaction, belonging to another defect, is present in the NaCl melt-grown crystal [Fig. 3(g)].[9,14] Also, other interactions in the melt-grown crystal can be associated with the latter defect and all these SHF interactions are identical to those of O(I).[14]

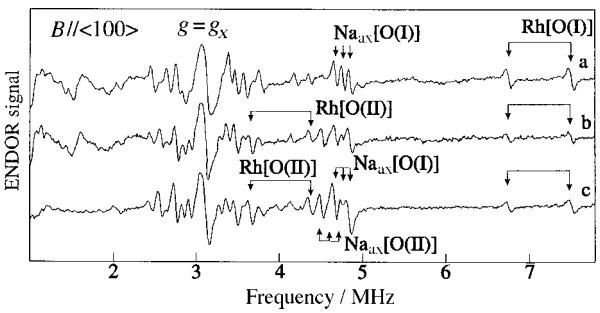

Fig. 4 X-Band ENDOR spectra for $B//\langle 100\rangle$ and $g = g_z$[O(II)] for the ^{23}Na and ^{103}Rh interactions: (a) solution-grown NaCl crystal measured after X-irradiation at LNT, (b) solution-grown NaCl crystal measured after X-irradiation at LNT and pulse-annealed at $T = 240$ K, (c) melt-grown NaCl crystal prior to any treatment.

A comparison between the latter ENDOR spectrum [Fig. 3(g)] with the spectrum of the solution-grown NaCl crystal X-irradiated at LNT and pulsed-annealed at 240 K [Fig. 3(d)] shows that both are very similar and can be interpreted in terms of O(I) and O(II). The latter similarity is confirmed by the mutually equal sodium and rhodium interactions (Fig. 4). To check the surprising presence of the overcompensated O(I) defect in melt-grown crystals, W-band EPR measurements were undertaken, as shown in Fig. 5: the O(I) spectrum can be clearly observed together with the O(II) lines. Moreover, for $B//\langle 100\rangle$ very small signals of the $g_\perp$ value of RTAX can be observed. The g-values of O(I) and RTAX determined from these W-band measurements are, within the experimental error, identical to those in the solution-grown NaCl crystal (Table 2). The g_z-value of these two defects could not be determined because of their low concentration, and even in W-band the EPR spectra around g_z are partly covered by those of O(II). It was again found impossible to change the relative intensities of the ENDOR spectra of O(I) and O(II) by heating or X-irradiation of the melt-grown crystal.[14] The same equilibrium ratio for O(II)/O(I) of 3 : 1 was found. Because of the lower concentration of O(I) and the similar g-values of O(I) and O(II), in the X-band EPR spectra the O(I) spectrum is totally hidden under the spectrum of O(II) and only with X-band ENDOR[14] and W-band EPR could the O(I) complex be detected.

The melt-grown AgCl single crystal. In the melt-grown AgCl the ENDOR spectra for $B//\langle 100\rangle$ and $g = g_z$ [Fig. 3(h)] show the presence of only one axial chloride interaction (12 lines), corresponding to the fully charge-compensated O(II) complex [Fig. 1(b)].[3]

Stability and charge compensation of O(I), O(II) and RTAX in solution- and melt-grown NaCl and AgCl crystals

In the solution-grown NaCl crystal at room temperature the non-locally charge-compensated RTAX defect is stable while the overcompensated O(I) and the fully charge-compensated O(II) defect are only present in very low concentrations. This small concentration of O(I) complexes can be charge compensated by the RTAX defects, while the remaining RTAX defects can be charge compensated by, *e.g.* distant Na^+ vacancies or

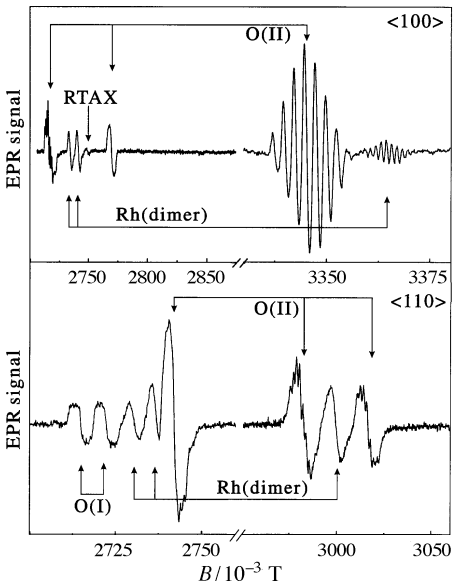

Fig. 5 W-Band EPR spectra for $B//\langle 100\rangle$ and $B//\langle 110\rangle$ of the melt-grown NaCl crystal doped with rhodium, measured at 20 K prior to any treatment.

OH^- groups. The latter are expected to be abundantly present in crystals grown from an aqueous solution.

In the melt-grown crystal, the same O(I), O(II) and RTAX defects are detected, but with a totally different stability. Although the vacancies are thought to be quite mobile at room temperature, the O(I) complexes and a very small concentration of RTAX are stable. In melt-grown crystals, containing few hydrogen groups, the small concentration of RTAX defects could be charge compensated by, *e.g.* a part of the abundantly present O(I) complexes or by distant Na^+ vacancies. The charge compensation of the O(I) complexes could occur by *e.g.* distant Cl^- vacancies.

The concentration ratio of O(I) to O(II) in both solution- and melt-grown NaCl crystals cannot be significantly changed by either heating, X-irradiation or any other treatment. This could indicate that there is an equilibrium between the O(I) and O(II) complexes. Neither in the solution-grown nor in the melt-grown crystal can the O(II) complex be isolated. It remains puzzling why, at room temperature, the essentially unstable O(I) defects in melt-grown NaCl crystals and the RTAX defects in solution-grown NaCl crystals are abundantly present.

Whereas in NaCl the O(II) defect is not detected without the presence of O(I), in AgCl no similar overcompensated $[RhCl_6]^{4-}$ defect is observed. From the comparison between the solution- and melt-grown NaCl crystals, the tentative conclusion for AgCl could be that in the solution-grown emulsion crystals the $[RhCl_6]^{4-}$ complexes[1,2] are less (*i.e* not) vacancy compensated than in melt-grown AgCl crystals.

Although experimentally very difficult, it seems important and interesting to check the vacancy compensation of the three Rh^{2+} complexes (R6, R5, R4) so far detected in AgCl emulsion crystals. R5 and R4 are assumed to have exchanged one and two Cl ligands for H_2O or OH^-, respectively.[1,2] For R5, R4 and even for the R6 $[RhCl_6]^{4-}$ centre the complex–vacancy configuration is still under investigation.

Conclusions

In this work the power of high resolution methods, *i.e.* X-band ENDOR and W-band EPR, has been demonstrated on Rh^{3+} doped NaCl crystals. The presence of two, one or zero vacancy compensated complexes has been monitored for different treatments of solution- and melt-grown crystals. In the latter, overcompensated Rh^{2+} centres are abundantly present whereas only a very small concentration of non-compensated Rh^{2+} complexes is observed. The opposite was found for solution-grown crystals where it seems that local vacancy compensation does not occur. Extrapolating this hypothesis to the photographically important AgCl emulsion crystals, this could mean that the uncompensated $[RhCl_6]^{4-}$ complex is dominant in microcrystals exposed to light. The present study demonstrated that high resolution magnetic resonance methods are of great potential value for the complicated study of relevant cation doped AgCl powder samples.

Acknowledgement

We thank FWO (Fonds voor Wetenschappelijk Onderzoek), IIKW (Interuniversitair Instituut voor Kernwetenschappen), IWT (Vlaams Instituut voor de bevordering van het wetenschappelijk-technologisch onderzoek in de industrie, "Flemish Institute for the Encouragement of Scientific and Technological Research in Industry"), K. S. and H. V., and Agfa-Gevaert NV for financial support.

References

1 H. Vercammen, T. Ceulemans, D. Schoemaker, P. Moens and D. Vandenbroucke, *Proceedings of the IS&T's 49th Annual Conference, Minneapolis*, 19–24 May 1996, 54.
2 P. Moens, H. Vercammen, D. Vandenbroucke, F. Callens and D. Schoemaker, *Proceedings of the IS&T's 49th Annual Conference, Minneapolis*, 19–24 May 1996, 56.
3 M. T. Olm, J. R. Niklas, J. M. Spaeth and M. C. R. Symons, *Phys. Rev. B*, 1988 **38**, 4343.
4 J. Wilkins, D. P. De Graag and J. N. Helle, *Phys. Lett*., 1965 **19**, 178.
5 R. S. Eachus and R. E. Graves, *J. Chem. Phys*., 1973, **59**, 2160.
6 R. S. Eachus and R. E. Graves, *J. Chem. Phys*., 1974, **61**, 2860.
7 N. M. Pinhal and N. V. Vugman, *J. Phys. C, Solid State Phys*., 1985, **18**, 6273.
8 L. Van Robbroeck, PhD Thesis, University of Antwerp, 1985.
9 S. Schweizer and J. M. Spaeth, *J. Phys. Chem. Solids*, 1997, **58**, 859.
10 M. Zdravkova, H. Vrielinck, F. Callens, E. Boesman, H. Vercammen and D. Schoemaker, *J. Appl. Phys*., 1997, **82**, 2476.
11 J. R. Shock and M. T. Rogers, *J. Chem. Phys*., 1975, **62**, 2640.
12 F. Callens, H. Vrielinck, P. Matthys, M. Zdravkova, H. Vercammen and D. Schoemaker, *J. Appl. Phys*., 1998, **84**, 428.
13 H. Vercammen, D. Schoemaker, H. Käß, E. Goovaerts, A. Bouwen, H. Vrielinck and F. Callens, *J. Appl. Phys*., 1998, **84**, 428.
14 K. Sabbe, F. Callens and E. Boesman, *Appl. Magn. Reson*., submitted for publication.
15 H. Vercammen, E. Goovaerts, H. Käß, A. Bouwen and D. Schoemaker, *J. Chem. Soc., Faraday Trans*., submitted for publication.
16 H. Vrielinck, F. Callens, M. Zdravkova and P. Matthys, *J. Chem. Soc., Faraday Trans*., in press.
17 H. Vercammen, T. Ceulemans, D. Schoemaker, F. Callens and D. Vandenbroucke, *J. Appl. Phys*., submitted for publication.
18 D. Schoemaker, *Phys. Rev. B*, 1973, **7**, 786.
19 S. V. Nistor, M. Velter Stefanescu and D. C. Mateescu, *Solid State Commun*., 1985, **53**, 989.

Paper 8/03049I